Electronic Supplementary Material (ESI) for Physical Chemistry Chemical Physics

Improving O_2 Production of WO_3 Photoanodes with IrO_2 in Acidic Aqueous Electrolyte

Joshua M. Spurgeon*, Jesus M. Velazquez, and Matthew T. McDowell

Joint Center for Artificial Photosynthesis
California Institute of Technology
Division of Chemistry and Chemical Engineering
1200 E. California Blvd. m/c 132-80
Pasadena, CA 91125 (USA)

Supporting Information

Electrode Illumination Schematic.

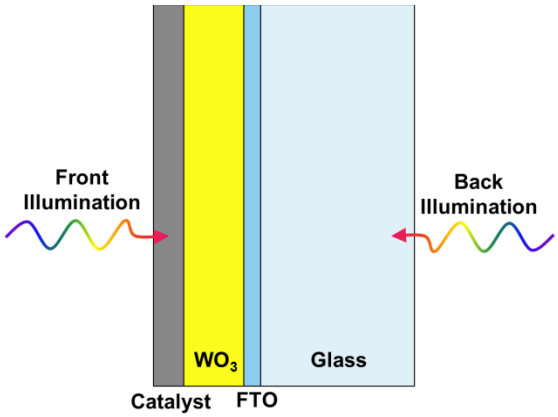

Figure S1. Schematic for OER catalyst/WO_3/FTO/glass photoanodes. Under front illumination conditions, the light was passed through the catalyst layer before getting to the photoactive WO_3. Under back illumination conditions, the light passed through the highly transparent glass substrate and FTO back contact before absorption in the WO_3 layer, without first passing through the catalyst.

IrO_2 on WO_3 Contact.

a)

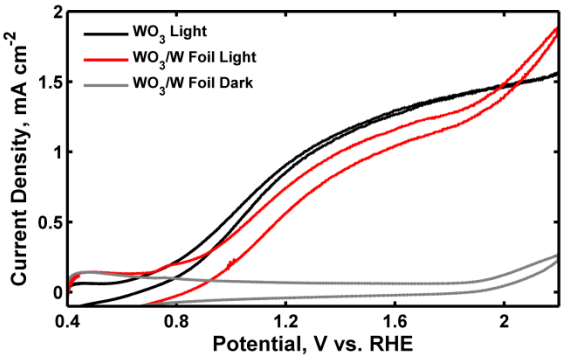

b)

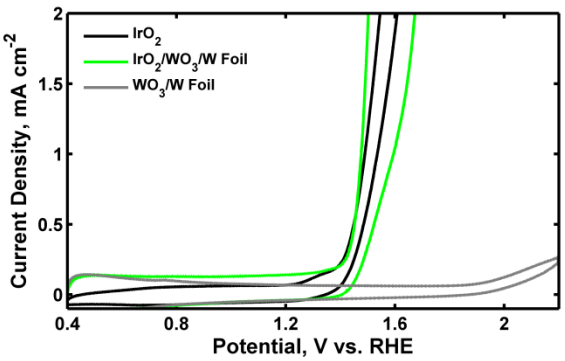

Figure S2. *J-E* behavior for WO_3 on W foil. Photoelectrochemical current-density (*J*) vs. potential (*E*) behavior in 1 M H_2SO_4 for (a) front-illuminated (black line) WO_3 on FTO, (red line) front-illuminated WO_3 on W foil, and (gray line) WO_3 on W foil in the dark. (b) Dark *J-E* behavior for (black line) sputtered IrO_2 on FTO, (green line) sputtered IrO_2 on WO_3/W foil, and (gray line) WO_3/W foil.

To ensure that the electrocatalytic current observed on WO_3 photodiodes in reverse bias at > 1.4 V vs. RHE was not due to a shunt caused by IrO_2 deposited directly in contact with the FTO substrate, WO_3 on W foil electrodes were fabricated. By annealing these electrodes in air at 400 °C for 2 hr, all exposed substrate at the bottom of the nanopores and cracks in the bulk WO_3 was oxidized to WO_3 as well. This was demonstrated by the lack of shunting in an electrolyte with a fast, one-electron redox couple (Fig. 1). During sputtering of IrO_2, a mask was used to deposit the catalyst only on the WO_3 film to avoid any contact with the W foil or any edge effects. Nevertheless, as demonstrated in Figure S2b, sputtered IrO_2/WO_3/W foil electrodes displayed electrocatalytic current similar to IrO_2 by itself. The shunt therefore was interpreted to occur through the WO_3 layer.

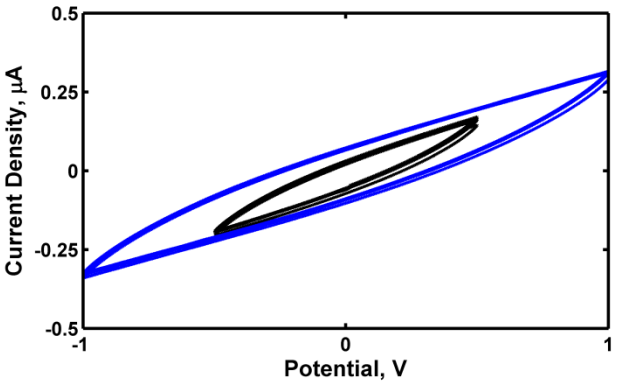

Figure S3. Solid-state cyclic voltammogram for IrO_2 contacts on WO_3. Current vs. voltage (*I-V*) behavior for two-electrode CV sweeps at 100 mV s^{-1} using sputtered IrO_2 contact pads 1 mm apart on WO_3 on glass (without FTO), scanning from (black lines) -0.5 to 0.5 V and from (blue lines) -1.0 to 1.0 V.

To verify the finding of ohmic behavior between the IrO_2 catalyst and WO_3 semiconductor, an attempt was made to directly investigate the nature of the contact with a solid-state measurement. WO_3 was deposited on a cleaned glass slide without an underlying transparent conductive layer, then two IrO_2 contact pads were deposited on the WO_3 by sputtering for 30 min using a mask to define square spots spaced 1 mm apart. A coiled Cu wire was attached to each IrO_2 spot with Ag paint, and these wires were used in two-electrode cyclic voltammograms at various scan rates and potentials. As shown in Figure S3, the resulting currents were low (in the µA range) due to the high resistance of the WO_3 layer. Hysteresis in the data was ascribed to capacitance in the WO_3 layer. Still, the overall trend across a 2 V range was quite linear, an indication of ohmic behavior.

Co_3O_4 and RuO_2 Catalyst Layers.

In addition to IrO_2, the OECs Co_3O_4 and RuO_2 were tested as drop-casted, sintered films and as sputtered films. Due to their instability in the 1 M H_2SO_4 electrolyte used in this work, they were not explored further.

For the drop-cast, sintered catalyst electrodes, three different oxygen-evolving metal oxide catalysts (IrO_2, RuO_2, or Co_3O_4) were separately deposited onto thin WO_3 films by drop-casting solutions of metal salts and then sintering to achieve the oxide form. A micropipette was used to drop-cast 20 µL of a 20 mM solution of the corresponding metal salt ($IrCl_3 \cdot 3H_2O$ from Fisher Scientific, $RuCl_3 \cdot xH_2O$ from Alfa Aesar, or $Co(NO_3)_2 \cdot 6H_2O$ from Alfa Aesar) in isopropanol on a ~1 cm^2 area of the WO_3. These films were allowed to dry at room temperature for ~ 1 hr then sintered at 400 °C in air for 1 hr. Analogous electrodes of the OEC directly on FTO glass were produced by the same method.

For the sputtered catalyst electrodes, OEC films of IrO_2, RuO_2, or Co_3O_4 were sputtered from metal targets of Ir, Ru, or Co (all ≥ 99.9% from AJA International), respectively. In each case, the catalyst layer was sputtered onto the WO_3 film from an RF source at 200 W at 300 °C under a constant flow of 3.0/3.0 sccm Ar/O_2 for IrO_2 and 4.5/0.5 sccm Ar/O_2 for RuO_2 and Co_3O_4 while maintaining an overall pressure of 6 mtorr. Two different thicknesses of each catalyst were produced by sputtering for either 0.5 min (< 10 nm) or 30 min (> 100 nm). Analogous electrodes of the OEC directly on FTO glass were produced by the same method.

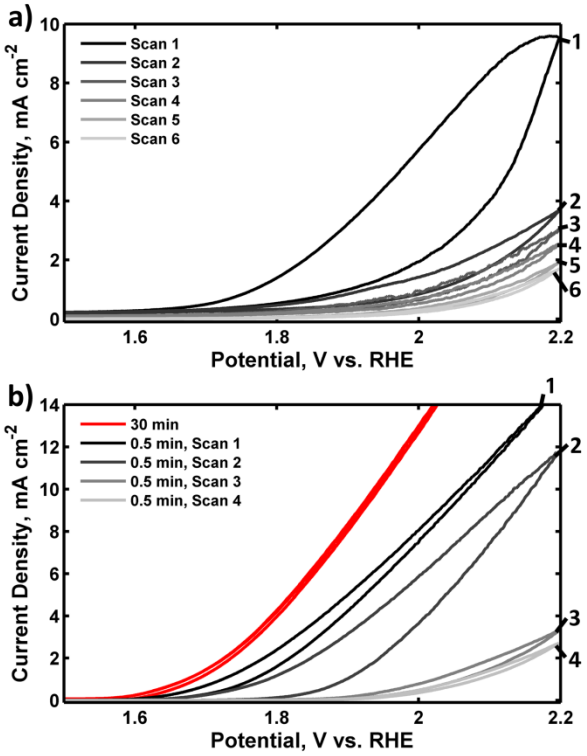

Figure S4. Instability of Co_3O_4 during cyclic voltammetry. *J-E* behavior in 1 M H_2SO_4 of (a) sintered Co_3O_4 on WO_3 over 6 scans, and (b) sputtered Co_3O_4 on FTO/glass over 4 scans. Thin, 0.5 min sputtered Co_3O_4 decayed rapidly over 4 scans (black to gray lines). Although thick, 30 min sputtered Co_3O_4 (red line) appeared stable over 4 scans, the current decayed away after extended use (> 1 hr) in 1 M H_2SO_4.

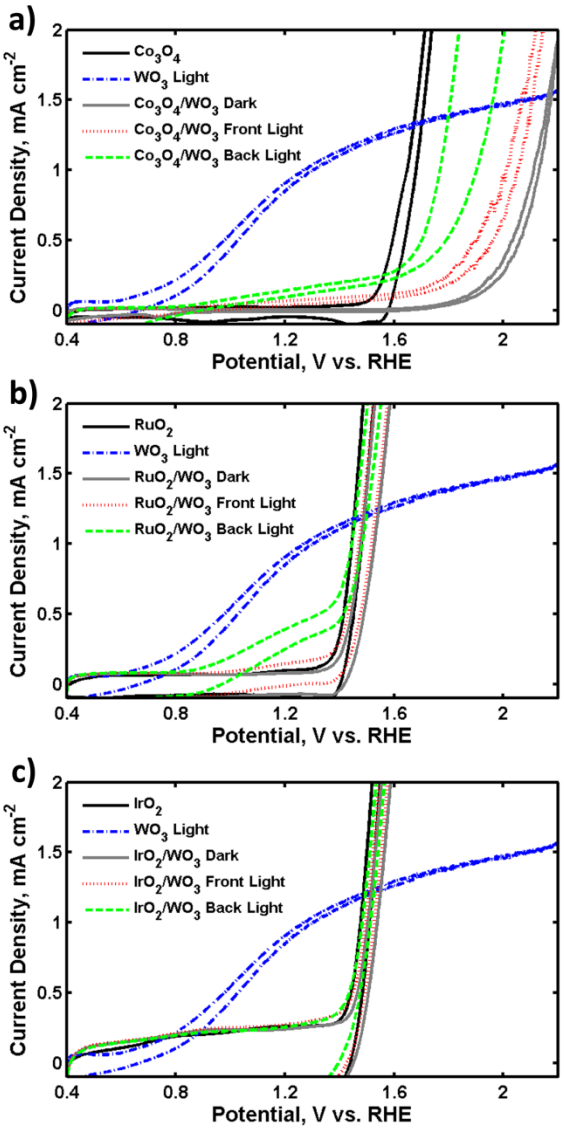

Figure S5. *J-E* behavior for drop-cast, sintered OER catalysts on WO_3. Photoelectrochemical current-density (*J*) vs. potential (*E*) behavior in 1 M H_2SO_4 for (a) Co_3O_4, (b) RuO_2, and (c) IrO_2 sintered from drop-cast metal salt solutions on WO_3 thin films and annealed in air at 400 °C for 1 hr. Performance is shown for (green lines) back illumination, (red lines) front illumination, and (gray lines) in the dark, with (blue lines) bare WO_3 under illumination and (black lines) the catalyst by itself in the dark for reference.

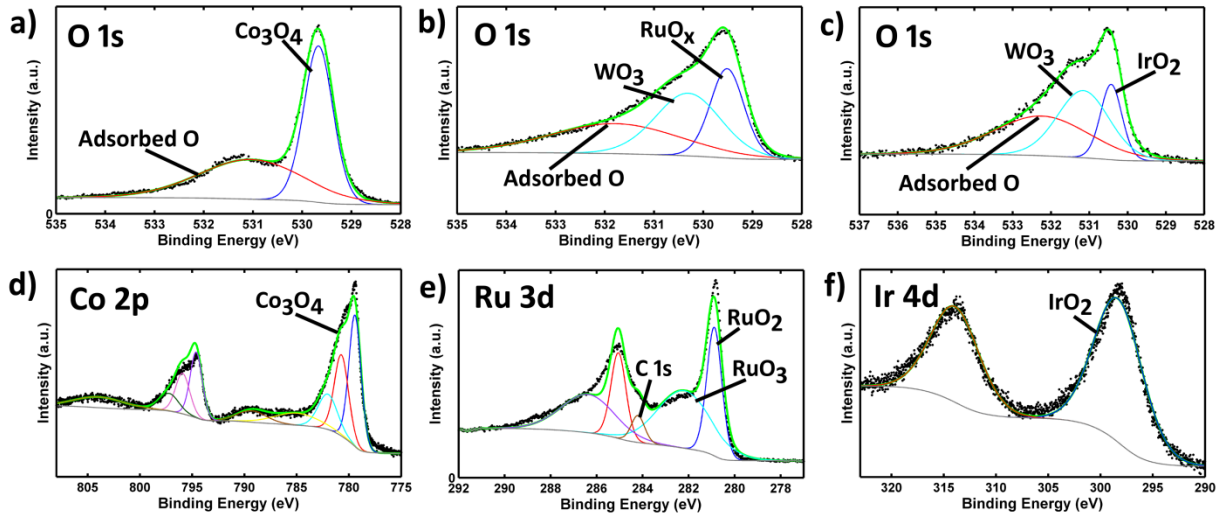

Figure S6. XPS of sputtered OER catalyst films on WO_3 photoanodes. High resolution scans for sputtered (a,d) Co_3O_4, (b,e) RuO_2, and (c,f) IrO_2 on WO_3 thin films. The (a-c) O 1s, (d) Co 2p, (e) Ru 3d, and (f) Ir 4d regions are shown. The RuO_2 and IrO_2 films were sputtered for 0.5 min, but the Co_3O_4 film was sputtered for 30 min to obtain a better Co 2p signal for clearer peak fitting.

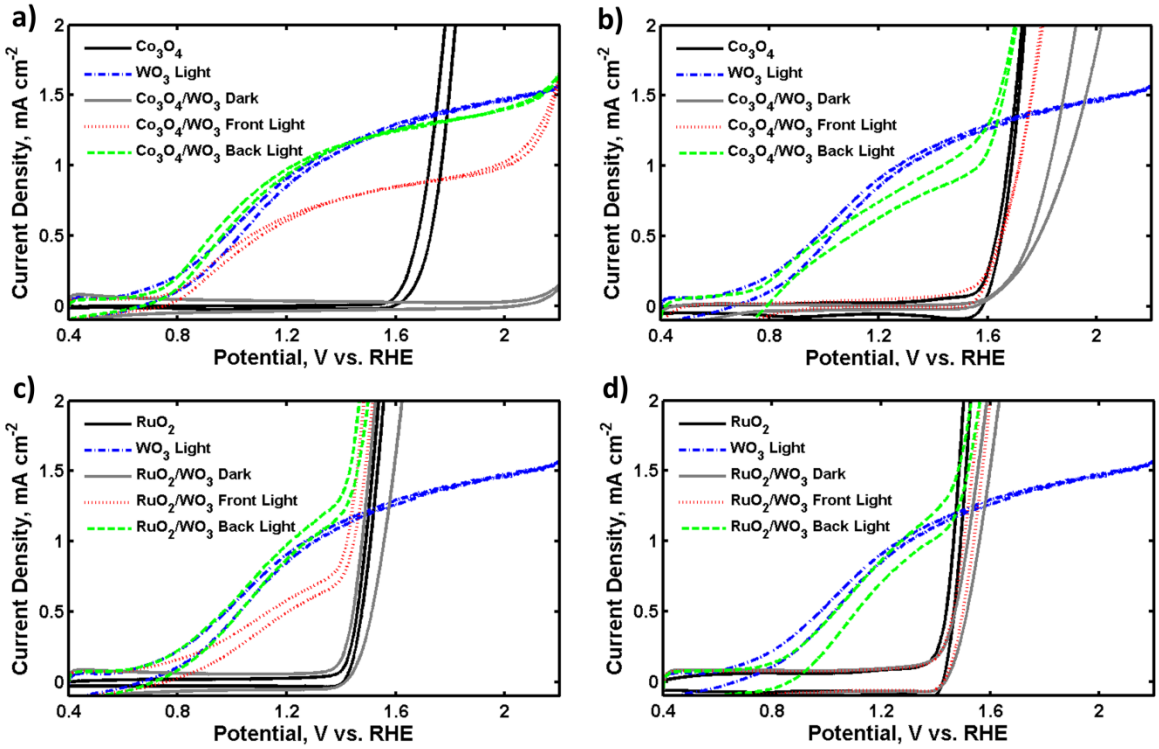

Figure S7. *J-E* behavior for sputtered OER catalyst on WO_3. Photoelectrochemical current-density (*J*) vs. potential (*E*) behavior in 1 M H_2SO_4 for (a,c) 0.5 min sputtered and (b,d) 30 min sputtered films of (a,b) Co_3O_4, and (c,d) RuO_2 on WO_3. Performance is shown for (green lines) back illumination, (red lines) front illumination, and (gray lines) in the dark, with (blue lines) bare WO_3 under illumination and (black lines) the catalyst by itself in the dark for reference.

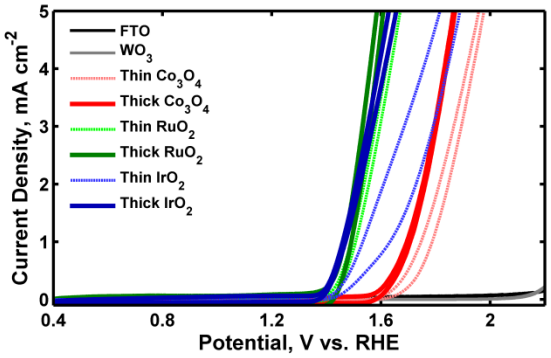

Figure S8. Dark *J*-*E* behavior for sputtered OER catalysts. Dark electrochemical current-density (*J*) vs. potential (*E*) behavior in 1 M H_2SO_4 for (black) FTO, (gray) WO_3, (light red, dashed) thin sputtered Co_3O_4, (dark red) thick sputtered Co_3O_4, (light green, dashed) thin sputtered RuO_2, (dark green) thick sputtered RuO_2, (light blue, dashed) thin sputtered IrO_2, and (dark blue) thick sputtered IrO_2.

Optical Transmittance for Sintered and Sputtered IrO_2 Layers.

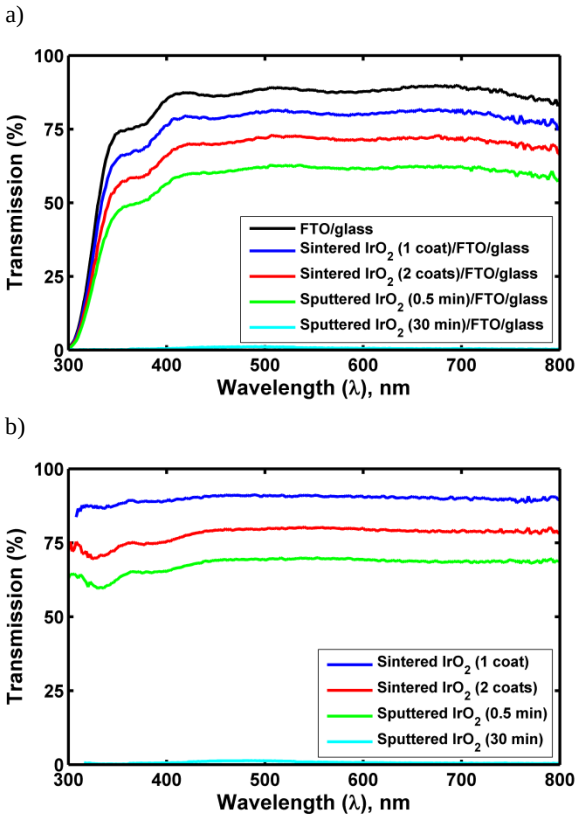

Figure S9. Optical transmission of IrO_2 catalyst layers. The percent of light transmitted vs. wavelength for sintered and sputtered IrO_2 layers on (a) FTO/glass substrates and (b) baseline-corrected for FTO/glass substrates to determine transmission only through the IrO_2 layer.

Annealing Sputtered IrO_2/WO_3 Photoanodes.

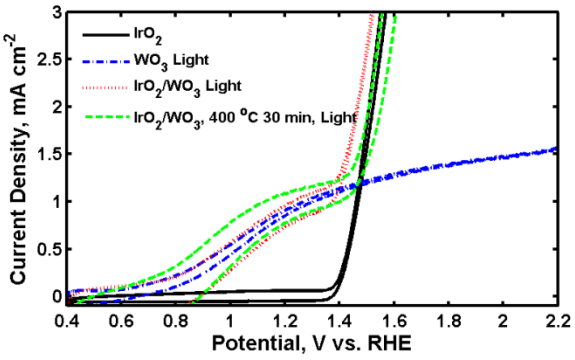

Figure S10. *J-E* behavior for annealed, sputtered IrO_2 on WO_3. Photoelectrochemical current-density (*J*) vs. potential (*E*) behavior in 1 M H_2SO_4. Performance is shown for 30 min sputtered IrO_2/WO_3 (red lines) as-deposited and (green lines) annealed under back illumination, with (blue lines) bare WO_3 under illumination and (black lines) the catalyst by itself in the dark for reference. Annealed samples were heated in air at 400 ºC for 30 min.

IrO_2 Catalyst Layer Morphology.

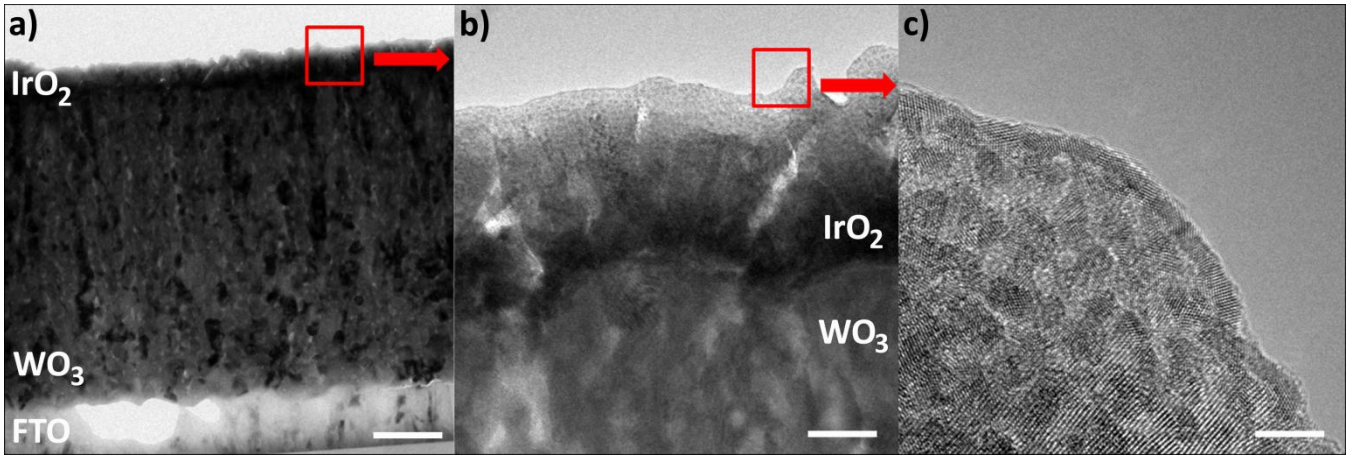

Figure S11. Morphology of sputtered IrO_2 layer. Cross-sectional TEM images for 30 min sputtered IrO_2 on WO_3 with a scale bar of (a) 200 nm, (b) 30 nm, and (c) 5 nm.

O_2 Production Measurements.

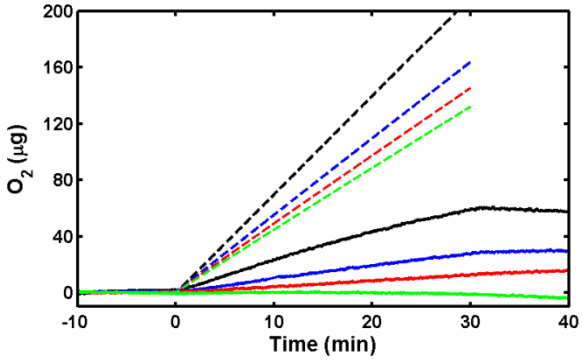

Figure S12. O_2 production of a bare WO_3 photoanode. The amount of O_2 produced by a bare, sputtered WO_3 film in 1 M H_2SO_4 under illumination while biased at a given potential, as determined by (dashed lines) the total charge passed (assuming 100% faradaic conversion to O_2) and by (solid lines) an optical O_2 sensor. The WO_3 photoanode was biased at potentials of (green lines) 1.4 V, (red lines) 1.5 V, (blue lines) 1.6 V, and (black lines) 2.0 V vs. RHE.

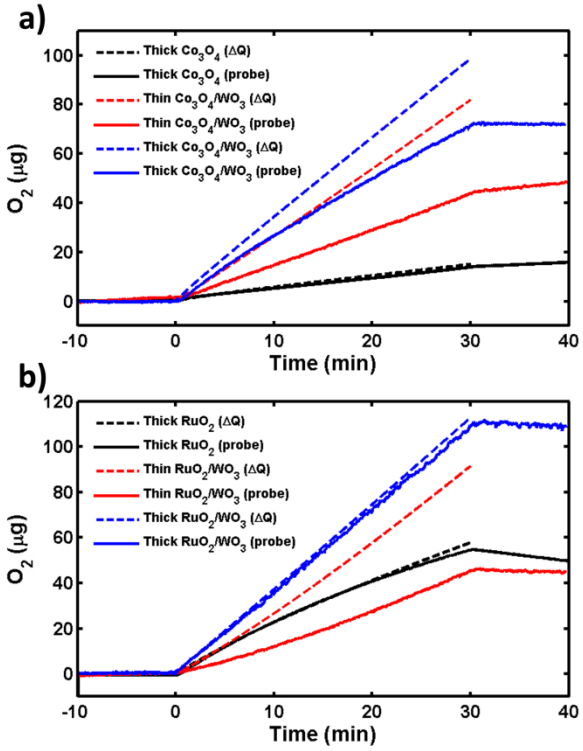

Figure S13. O_2 production of sputtered OER catalysts on WO_3. The amount of O_2 produced at 1.2 V vs. RHE under back illumination in 1 M H_2SO_4 for a WO_3 photoanode with a sputtered catalyst film of (a) Co_3O_4, and (b) RuO_2. The quantity of O_2 was determined by (dashed lines) the total charge passed (assuming 100% faradaic conversion to O_2) and by (solid lines) an optical O_2 sensor. For catalyst thicknesses, (red lines) a thin film was sputtered for 0.5 min, and (blue lines) a thick film was sputtered for 30 min. To demonstrate the high faradaic efficiency achievable with each catalyst, (black lines) bare catalyst films were measured in the dark at 1.5 V vs. RHE (RuO_2) or 1.7 V vs. RHE (Co_3O_4).

Electrode Stability.

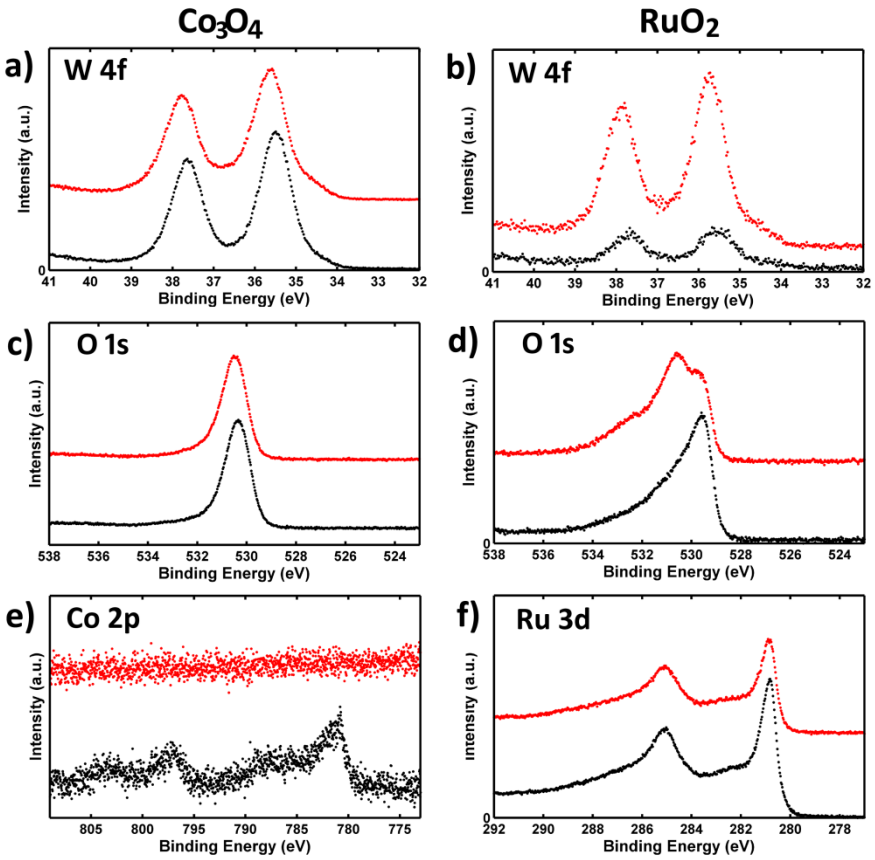

Figure S14. XPS of sputtered OER catalysts on WO_3. High resolution XPS spectra for WO_3 films covered with (a, c, e) Co_3O_4, and (b, d, f) RuO_2, each sputtered for 0.5 min. The regions shown are (a,b) W 4f, (c,d) O 1s, (e) Co 2p, and (f) Ru 3d. The films were analyzed (black lines) as-deposited, and (red lines) after a *J-E* behavior measurement under illumination in 1 M H_2SO_4.

Figure S14 shows the XPS spectra for thin, 0.5 min sputtered OEC/WO_3 electrodes in which the catalyst layer was thin enough to allow sampling of the underlying WO_3. As expected from the decay in current observed during *J-E* measurements (Fig. S4), the Co_3O_4 Co 2p signal is completely gone after measurement in 1 M H_2SO_4 (Fig. S14e). Although the catalytic current with RuO_2 was much steadier, the XPS results reveal that this OEC was not long-term stable in strong acid either. After measuring the *J-E* behavior, the W 4f peaks of the RuO_2/WO_3 sample became more intense (Fig. S14b) and the O 1s peak changed such that the WO_3 component became more prominent relative to the RuO_x component (Fig. S14d and Fig. S6b), indicating the gradual dissolution of the RuO_2 layer.

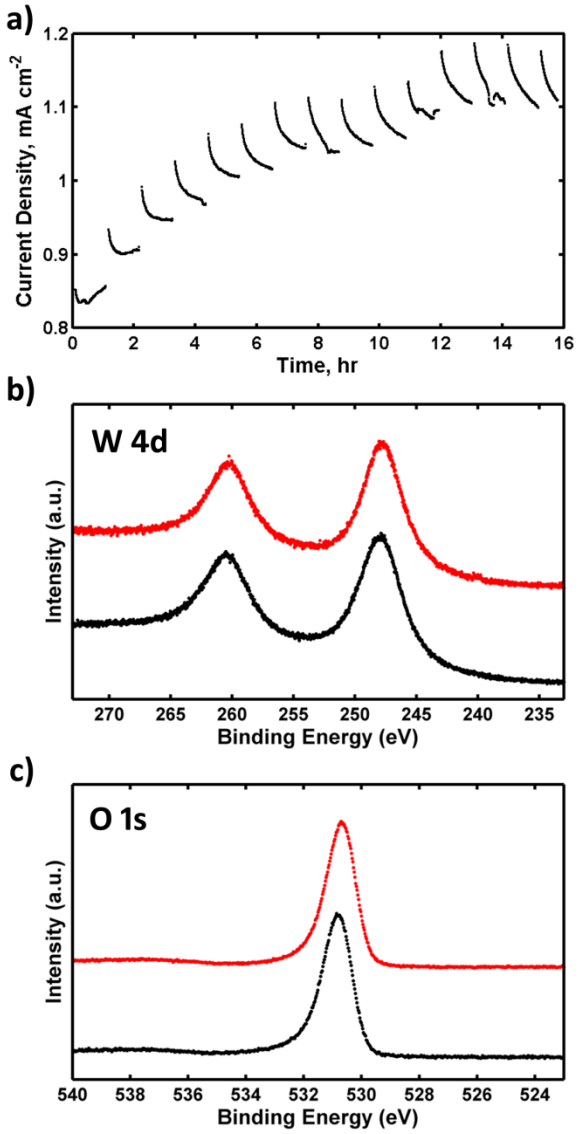

Figure S15. Stability of WO_3 photoanodes. (a) Current density vs. time measurement for bare WO_3 in 1 M H_2SO_4 under 1 sun AM1.5 illumination at 1.2 V vs. RHE with cyclic voltammetric (CV) measurements (30 mV s^{-1} scan from 0.4 to 2.0 V vs. RHE and back, 2 scans) made every hour. The discontinuities in the curve are due to the CV measurements. (b, c) XPS data for sputtered WO_3 films (black lines) as-deposited and (red lines) after 12 hr at 1.2 V vs. RHE in 1 M H_2SO_4 under 1 sun AM1.5 illumination showing high resolution scans of (b) the W 4d region and (c) the O 1s region.

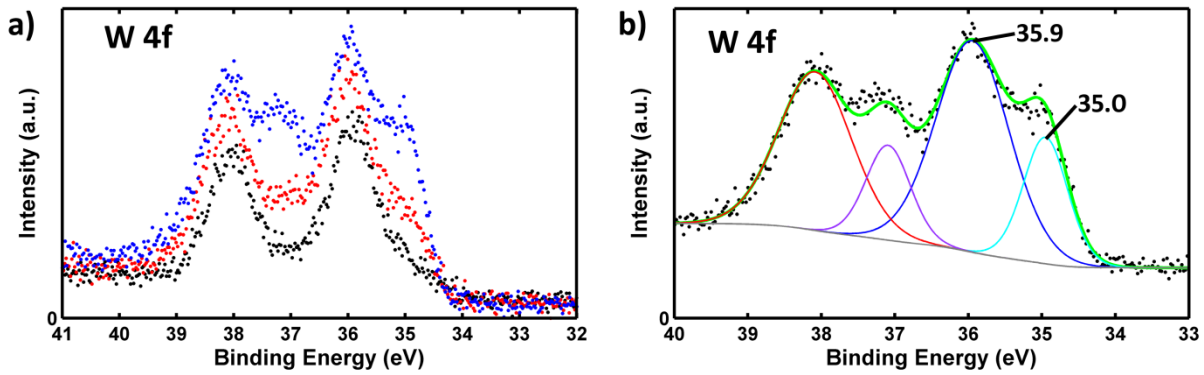

Figure S16. Stability of sputtered IrO_2 on WO_3. XPS spectra of the W 4f region of thin, 0.5 min sputtered IrO_2 on WO_3, showing (a) the sequential change from (black lines) as-deposited to (red lines) after a *J-E* behavior measurement under illumination in 1 M H_2SO_4, to (blue lines) after 12 hr at 1.2 V vs. RHE under illumination in 1 M H_2SO_4. Also shown are (b) the fitted peaks for the sample after 12 hr at 1.2 V vs. RHE under illumination in 1 M H_2SO_4.

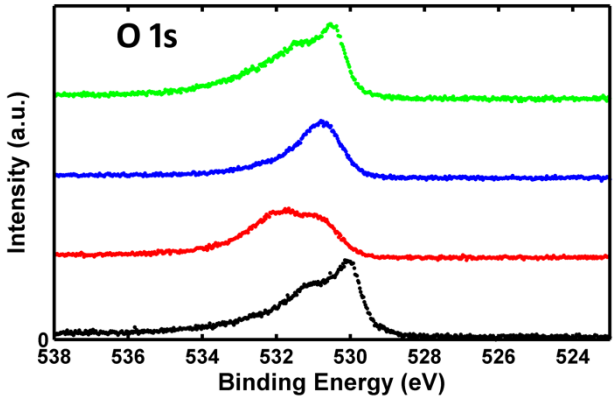

Figure S17. XPS comparison of different IrO_2 deposition methods. XPS spectra of the O 1s region of WO_3 with IrO_2 deposited on it by (black line) drop-casting an $IrCl_3$ solution and then sintering at 400 °C for 1 hr, (red line) electrodeposition, (blue line) electrodeposition followed by a 400 °C anneal for 1 hr, and (green line) sputtering for 0.5 min.

Electrodeposited IrO_2 on WO_3 Photoanodes.

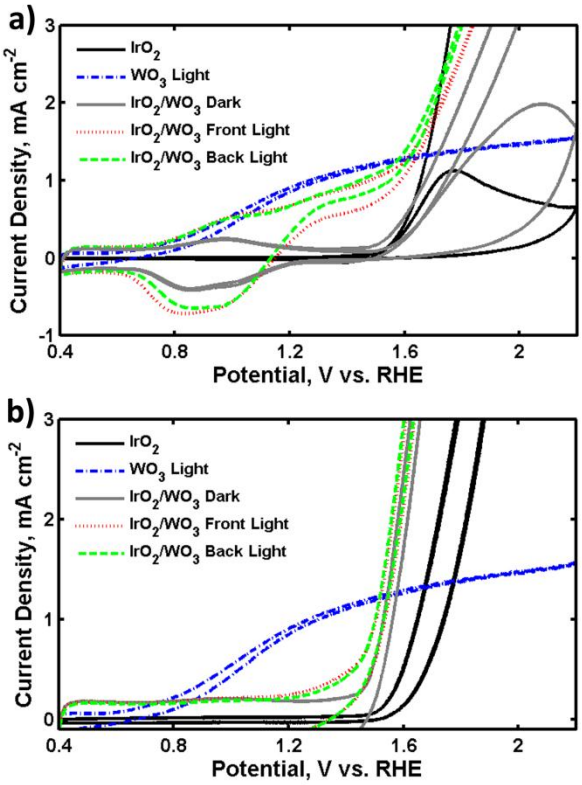

Figure S18. *J-E* behavior for electrodeposited IrO_2 on WO_3 by the method of Zhao et al.[1] Photoelectrochemical current-density (*J*) vs. potential (*E*) behavior in 1 M H_2SO_4 for electrodeposited IrO_2 on WO_3 (a) as-deposited and (b) after a 400 °C anneal for 1 hr. Performance is shown for (green lines) back illumination, (red lines) front illumination, and (gray lines) in the dark, with (blue lines) bare WO_3 under illumination and (black lines) the catalyst by itself on FTO in the dark for reference. Multiple successive scans of IrO_2/WO_3 in the dark and IrO_2 on FTO are included to demonstrate unstable current in (a) and stable current in (b).

For this IrO_2 electrodeposition procedure, colloidal IrO_x in a pH 1 mixture was prepared as published.[1] The solution was stored in a refrigerator at 4 °C. IrO_x films were deposited on FTO/glass and on WO_3 by maintaining the potential at 1.4 V vs. Ag/AgCl until 2.5 C of charge had been passed. In each case, the exposed area of the working electrode for deposition was 1 cm^2. During deposition, the solution was stirred vigorously and kept in an ice bath.

Drop-cast, Particulate IrO_2 on WO_3 Photoanodes. Another method tested for IrO_2 catalyst attachment was the drop-casting of IrO_2 powders directly on the WO_3 surface. IrO_2 powder (99%, Alfa Aesar) was mixed to a 30% w/w IrO_2 suspension in isopropanol and then sonicated for > 3 hr before drop-casting 20 µL of the suspension onto a 1 cm^2 WO_3 electrode area using a micropipette and drying in ambient for ~ 1 hr. Eight sequential coatings of IrO_2 particles were applied. Some particulate IrO_2/WO_3 electrodes were also annealed at 500 °C for 2 hr in air. Analogous electrodes of IrO_2 particles directly on FTO glass were produced by the same method.

Before any annealing step, particulate IrO_2/WO_3 photoanodes performed comparably to bare WO_3 under back illumination, but with the photocurrent was reduced by 68% due to catalyst light absorption under front illumination (Table 1). However, these samples displayed no O_2 production and had issues with catalyst loss due to poor adhesion. After annealing to sinter the catalyst particles to the WO_3 surface, most IrO_2 particles remained attached during testing. A reduction in photocurrent was observed after the high temperature anneal, but the faradaic oxygen production efficiency increased from 0 to 43% (Table 1). Considering the relatively low O_2 yield compared to the percentage of photocurrent lost under front illumination, this catalyst attachment method was not pursued further. However, a more sophisticated technique to pattern IrO_2 particles at set dimensions to optimize catalytic activity relative to optical absorption may still hold promise for future studies.

1. Y. X. Zhao, E. A. Hernandez-Pagan, N. M. Vargas-Barbosa, J. L. Dysart and T. E. Mallouk, *J. Phys. Chem. Lett.*, 2011, **2**, 402-406.